Chapter 9

Phase Manipulation of Ultrashort Soft X-Ray Pulses by Reflective Gratings

Fabio Frassetto, Paolo Miotti and Luca Poletto

Additional information is available at the end of the chapter

http://dx.doi.org/10.5772/63416

Abstract

In this chapter, we discuss the use of reflective diffraction gratings to manipulate the phase of ultrashort pulses in the extreme ultraviolet (XUV) and soft X-ray spectral regions. Gratings may be used to condition the spectral phase of ultrashort pulses, e.g., to compensate for the pulse chirp and compress the pulse, similarly to what is routinely realized for visible and infrared pulses. The chirped pulse amplification technique has been already proposed for soft X-ray free-electron laser radiation; however, it requires the use of a compressor to compensate for the pulse chirp and get closer to the Fourier limit. There are fundamental differences when operating the gratings at wavelengths shorter than ≈40 nm on a broad band: (a) the gratings are operated at grazing incidence; therefore, the optical design has to be consequently tailored to this peculiar geometry; (b) the grating efficiency is definitely lower; therefore, the number of diffractions has to be limited to two. We discuss the different configurations that can be applied to the realization of a grating stretcher/compressor.

Keywords: diffraction gratings, ultrafast optics, extreme ultraviolet, soft X-ray optics, chirped pulse amplification

1. Introduction

XUV and X-ray radiations have been used for many fundamental discoveries and outstanding applications in natural sciences. It has played a crucial role in basic research, medical diagnostics, and industrial development. In particular, the impressive developments in laser technology over the last decades lead to the generation of XUV and X-ray coherent ultra-

short and ultra-intense pulses in the femtosecond and sub-femtosecond time scale (1 fs = 10^{-15} s) [1–3]. Ultrafast short-wavelength radiation offers the unique capability to access and measure the structural arrangement and electronic structure inside the nucleus [4, 5]. The main available tools to generate ultrashort coherent pulses are presently high-order laser harmonics generated in gas and free-electron lasers [6].

High-order harmonics (HHs) are generated through the interaction between an ultrashort laser pulse and a gas in a cell or in a jet. Because of the strong peak power of the femtosecond laser pulse, a nonlinear interaction with the gas takes place and produces odd laser harmonics that may easily extend well above the order of several tens. The HH spectrum is described as a sequence of peaks corresponding to the odd harmonics of the fundamental laser wavelength and having an intensity distribution characterized by a plateau whose extension is related to pulse intensity and frequency. The use of advanced phase-matching mechanisms and interaction geometries has made possible the generation of HHs in the water window region between 2.3 and 4.4 nm, while still using a table-top laser source [7–9]. The radiation generated with the scheme of the HHs using few-optical-cycle laser pulses is currently the main tool for the investigation of matter with attosecond resolution (1 as = 10^{-18} s) [10–13]. Both trains [14, 15] and isolated [16–19] bursts of attosecond pulses have been experimentally demonstrated. The physical background of ultrashort pulses originates from the model of HH generation, i.e., the phase-matched emission of radiation results from the recombination of a tunnel-ionized electron with its parent ion. Once the conditions for such recombination are realized in only one occurrence per laser pulse, an isolated pulse is generated. Both trains and isolated attosecond pulses are positively chirped, resulting from the different duration of the quantum paths that contribute to the emitted spectrum [20]. Due to the nonzero chirp, the pulse temporal duration is longer than the Fourier limit. Positively chirped pulses may be temporally compressed by introducing a system that gives a compensating negative chirp. The compression has been achieved using a thin metallic filter with negative group-delay dispersion (GDD) as discussed in Refs. [15, 17] or broadband multilayer-coated optics with aperiodic layers [21].

Free-electron laser (FEL) sources generate radiation in the XUV and X-ray spectral regions with high spatial coherence, ultrashort time duration, and an increase of 6–8 orders of magnitude on the peak brilliance with respect to third-generation synchrotrons. FEL operation relies on a relativistic electron beam as the lasing medium which moves freely through a periodic magnetic structure (i.e., the undulator) that induces radiation [22]. There are presently four FEL user facilities operated at short wavelengths and dedicated to user-defined experiments: FLASH in Germany, SACLA in Japan, LCLS in USA, and FERMI in Italy. Presently, FEL pulses as short as 3 fs have been characterized at LCLS [23]. In order to increase the temporal resolution in pump-probe experiments, several approaches have been proposed for the generation of ultrashort FEL pulses in the femtosecond and sub-femtosecond regime, as the time slicing [24–26] or the reduction of the electron bunch charge [27]. Most of these methods rely on the selection of a small portion of the electron beam which undergoes FEL amplification, with a reduction of the amount of charge that contributes to the light amplification. A different possibility is the optical compression of the radiation pulse generated by

the whole electron beam that is required to have a nonzero energy chirp in order to generate a chirped pulse. As for optical lasers, where frequency chirping is introduced to stretch the pulse before its amplification and then compensated after amplification to recover the ultrashort duration and high peak power, chirped-pulse amplification (CPA) may also be applied to FELs [28, 29]. In case of seeded FELs, the seeding laser pulse has to be stretched in time before interacting with the electron beam. This solution allows the use of the whole electron beam charge obtaining a significantly higher number of photons.

Indeed, for both HH and FEL facilities, the availability of a compressor tunable in the spectral band of operation of the source, capable of changing the spectral phase of the pulses, is particularly attractive, either to compensate for the intrinsic chirp or to realize CPA.

Here we discuss the use of gratings at grazing incidence to realize a tunable device to manipulate the spectral phase of XUV and X-ray–chirped pulses. In designing instruments for photon handling in the XUV ultrafast domain, there are some basic differences with respect to the traditional optical schemes in the visible and infrared domain [30, 31]. The first is to exploit the very short duration of the pulse, the study of the optical length of the rays gathered by the pupil and their equalization is mandatory. Moreover, the very extended bandwidth of operation may be exploited only if the instrument has a rather flat spectral response. Finally, an overall high throughput of the instrument is often a crucial feature to maintain high peak intensity.

The use of gratings at grazing incidence to realize tunable monochromators for XUV ultrafast pulses is well established. Several monochromatic beamlines are presently in operation both with HHs [32–35] and FELs [36–39].

When using a grating for ultrafast pulses, the main problem faced with is the pulse-front tilt that is introduced by diffraction [40]. Indeed, each ray that is diffracted by two adjacent grooves is delayed by $m\lambda/c$, where m is the diffraction order, λ is the wavelength, and c is the speed of light in vacuum. The pulse-front tilt is given by the total difference in the optical paths of the diffracted beam, that is $\Delta\tau_G = m\lambda N/c$, where N is the total number of the illuminated grooves. This effect, that is totally negligible for picosecond or longer pulses, is noticeable in the femtosecond time scale, since it can dramatically degrade the instrumental ultrafast response. To overcome this effect, a double-grating configuration has to be adopted to compensate for the pulse-front tilt [41, 42]. The first grating is demanded to spectrally disperse the beam on an intermediate focal plane, where a slit performs the spectral selection, while the second grating compensates for the pulse-front tilt of the diffracted beam by equalizing the length of the optical paths. Double-grating instruments have been demonstrated to be very effective for HHs, with time resolution well below 10 fs [43–47]. Double-grating configurations, which are able to preserve the ultrafast duration of the pulse, have been also proposed as beam splitters for ultrafast intense pulses [48] and as infrared (IR)-XUV beam separators for HHs [49].

Here, we focus on the use of gratings to realize devices able to manipulate the spectral phase of chirped pulses, in particular to be used as XUV compressors.

2. Grating geometries for ultrashort pulses

Grazing incidence reflective gratings may be used either in the classical diffraction geometry (CDG) or in the off-plane geometry (OPG) [50].

The CDG is shown in **Figure 1(a)**. The grating equation is $\sin\alpha + \sin\beta = m\lambda\sigma_{CD}$, where α and β are, respectively, the incident and diffracted angles and σ_{CD} the groove density.

The OPG is shown in **Figure 1(b)**. The grating equation is $\sin\gamma\ (\sin\mu + \sin\nu) = m\lambda\sigma_{OP}$, where γ is the altitude angle, μ and ν are the azimuth angles as defined in the figure, and σ_{OP} is the groove density. The OPG, although seldom used, gives higher throughput than the classical mount, since it has been theoretically demonstrated and experimentally measured that the peak diffraction efficiency is close to the reflectivity of the coating at the altitude angle [51, 52]. Therefore, the OPG is suitable for the design of XUV grating instruments with high efficiency [53, 54].

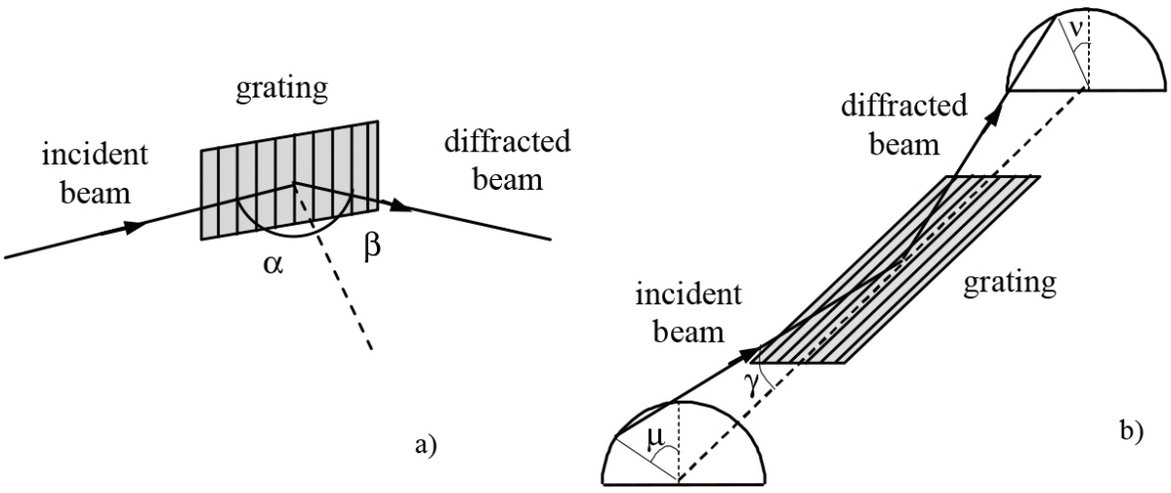

Figure 1. (a) Classical diffraction geometry; (b) off-plane geometry.

When realizing a grating compressor for ultrafast pulses, the main problem faced with is the pulse-front tilt given by the diffraction, as shown in **Figure 2** in the case of the CDG. Furthermore, different wavelengths are diffracted in different directions. The pulse-front tilt and the spectral angular dispersion have to be corrected by a second grating in a compensated configuration to fulfill the two following conditions: (1) the differences in the path lengths of rays with the same wavelength within the beam aperture that are caused by the diffraction from the first grating have to be compensated by the second grating; that is, the pulse-front tilt is corrected; (2) the angular spectral dispersion caused by the first grating has to be canceled by the second grating, that is, all the rays at different wavelengths exit the second grating with parallel directions. Both these conditions are satisfied by a scheme with two equal gratings mounted with opposite diffraction orders; that is, the incidence (incoming azimuth) angle on the second grating is equal to the diffraction angle (outcoming azimuth) from the first grating. The phase chirp introduced by the system is calculated as the difference in the optical

paths of rays at different wavelengths. This principle is well known for the realization of stretchers and compressors in the visible and near infrared [55, 56].

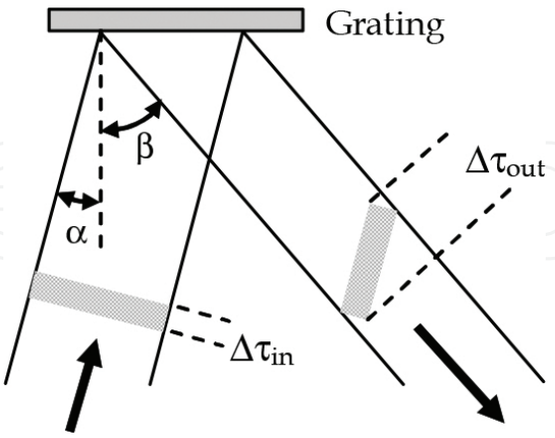

Figure 2. Pulse-front tilt of an ultrashort pulse diffracted by a grating in the CDG. $\Delta\tau_{in}$ and $\Delta\tau_{out}$ are the pulse duration at input and output, respectively. At the first diffracted order, the pulse-front tilt is $\Delta OP = N\lambda$, where N is the number of illuminated grooves.

3. Grazing incidence grating compressor

When applying the double-grating configuration to the phase manipulation of XUV pulses, all the optics have to be operated at grazing incidence. The simplest arrangement consists of two identical plane gratings mounted in the compensated configuration, as shown in **Figures 3** and **4**. Due to the symmetry of the configuration, the angular dispersion at the output is canceled, and the output rays are parallel to the input for all the wavelengths [57].

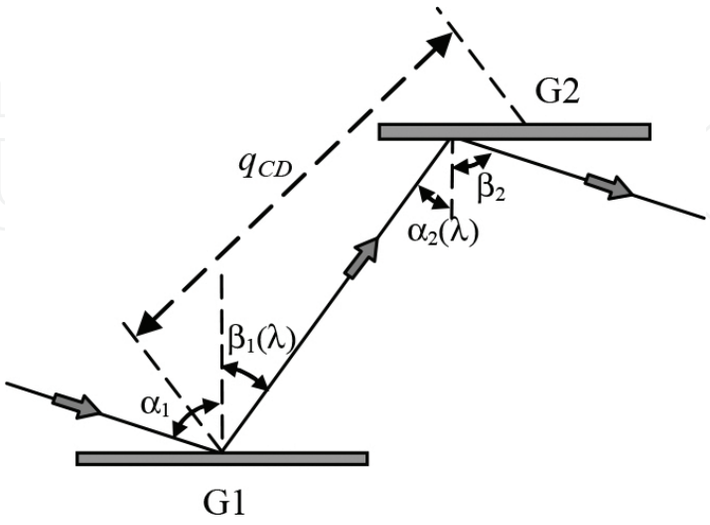

Figure 3. Double-grating compressor in the CDG. The diffraction angle from G2 is constant with the wavelength and equal to the incidence angle on G1, $\beta_2 = \alpha_1$.

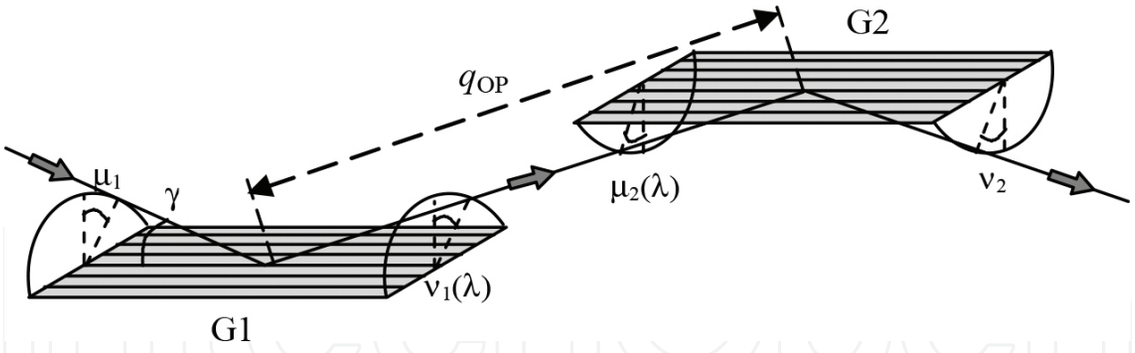

Figure 4. Double-grating compressor in the OPG. The outcoming azimuth from G2 is constant with the wavelength and equal to the incoming azimuth on G1, $\nu_2 = \mu_1$.

Since different wavelengths are diffracted by G1 at different angles, the rays do not make the same optical paths. In the case of the CDG, the optical path is analytically expressed (for less than a constant term) as

$$OP_{CD}(\lambda) = q_{CD}\frac{\cos\beta_c}{\cos\beta(\lambda)}\left[1-\sin\alpha\sin\beta(\lambda)\right] \tag{1}$$

where α is the incidence angle on G1, $\beta(\lambda)$ and β_c are, respectively, the diffraction angles from G1 at the generic wavelength λ and at the central wavelength of the interval of operation λ_c, and q_{CD} is the G1-G2 distance. The bandwidth of the pulse $\Delta\lambda$ is limited between λ_{min} and λ_{max}, $\Delta\lambda = \lambda_{max} - \lambda_{min}$, and $\underline{\lambda}_c = (\lambda_{min} + \lambda_{max})/2$. In case of a narrow-band pulse with $\lambda/\Delta\lambda < 20\%$, Eq. (1) is linearized in λ as

$$OP_{CD}(\lambda) = q_{CD}\lambda_c\left(\frac{m\sigma_{CD}}{\cos\beta_c}\right)^2\lambda \tag{2}$$

Similarly, in the case of the OPM, the optical path is expressed as

$$OP_{OP}(\lambda) = q\frac{\sin^2\gamma\cos\mu}{\cos\nu}\left(1+\sin\mu\sin\nu\right) \tag{3}$$

where μ is the incoming azimuth on G1 that has been chosen to have the central wavelength λ_c diffracted at $\nu_c = \mu$, i.e., $2\sin\gamma\sin\mu = \lambda_c\sigma_{OP}$, and q_{OP} is the G1-G2 distance. In case of a narrow-band pulse, Eq. (3) is linearized as

$$OP_{OP}(\lambda) = q_{OP}\lambda_c\left(\frac{m\sigma_{OP}}{\cos\mu}\right)^2\lambda \tag{4}$$

http://dx.doi.org/10.5772/63416

Note that in both cases the optical path increases with the wavelength, and this forces the group delay dispersion introduced by the double-grating configuration to be negative.

As usual, the group delay (GD) and the group delay dispersion (GDD) are expressed as a function of $\omega = 2\pi c/\lambda$: $GD(\omega) = \partial\varphi(\omega)/\partial\omega = OP(\omega)/c$ and $GDD(\omega) = \partial GD(\omega)/\partial\omega$. The central pulse frequency ω_c is defined as $\omega_c = 2\pi c/\lambda_c$.

For narrow-band pulses, the GD is also linear in frequency, and the GDD is constant and negative

$$GDD_{CD} = -\frac{q_{CD}c}{\omega_c^3}\left(\frac{2\pi\sigma_{CD}}{\cos\beta_c}\right)^2 \tag{5}$$

and

$$GDD_{OP} = -\frac{q_{OP}c}{\omega_c^3}\left(\frac{2\pi\sigma_{OP}}{\cos\mu}\right)^2 \tag{6}$$

Once the required GDD to manipulate the pulse has been defined, the above equations define the parameters of the grating compressor in both geometries.

Once the required GDD has been fixed, the two geometries give equivalent answer for $q_{OP}\,\sigma_{OP}^2/\cos^2\mu = q_{CD}\,\sigma_{CD}^2/\cos^2\beta_c$. In case of equal arms, i.e., $q_{OP} = q_{CD}$, since μ is typically below 20° and β_c above 80°, the groove density that would be required in the OPM is much higher than the CDM and may be not available from grating providers. Therefore, a compressor in the OPM is typically longer than the corresponding CDM, i.e., $q_{OP} > q_{CD}$.

The compressor introduces a spatial chirp of the pulse, i.e., rays with different wavelengths have the same output direction, but they are not exactly superimposed. In the conventional design of compressors for IR pulses, the spatial chirp is canceled by making the beam passing two additional times though the same gratings, so the output spatial dispersion is zero. This cannot be realized in grazing incidence, since it would require the insertion of two additional gratings that would make the configuration complex and inefficient. The spatial chirp $SC(\lambda)$ is expressed, in case of a narrow-band pulse, as

$$SC_{CD}(\lambda) = q_{CD}\sigma_{CD}\frac{\cos\alpha}{\cos^2\beta_c}\Delta\lambda \tag{7}$$

$$SC_{OP}(\lambda) = q_{OP}\sigma_{OP}\frac{1}{\cos^2\mu}\Delta\lambda \tag{8}$$

Since the rays are parallel, the spatial chirp does not influence the quality of the final spot size, since all the rays are focused on the same point.

In the following, we discuss the use of the double-grating configuration to the case of compression of FEL pulses and of attosecond pulses generated through HHs.

4. Grating compressor applied to FEL pulses

One of the main problems faced when manipulating intense FEL radiation is the use of robust optical components to be operated with the FEL pulses with minimum risk of damaging. From this point of view, grazing incidence elements are preferable. The double-grating compressor, whose optical elements are used at grazing incidence, is very suitable for FEL pulses. We assume FEL parameters already discussed in the literature [58] that may be a test case for the application to chirped-pulse amplification (CPA) of FEL pulses.

The scheme of the CPA applied to a seeded FEL is shown in **Figure 5**. The electron beam, being generated through a chirped laser seeding pulse, originates, after the radiator, a chirped optical pulse with positive GDD. The chirp is corrected by the grating compressor that introduces different optical paths for different wavelengths and shortens the pulse duration close to the Fourier limit.

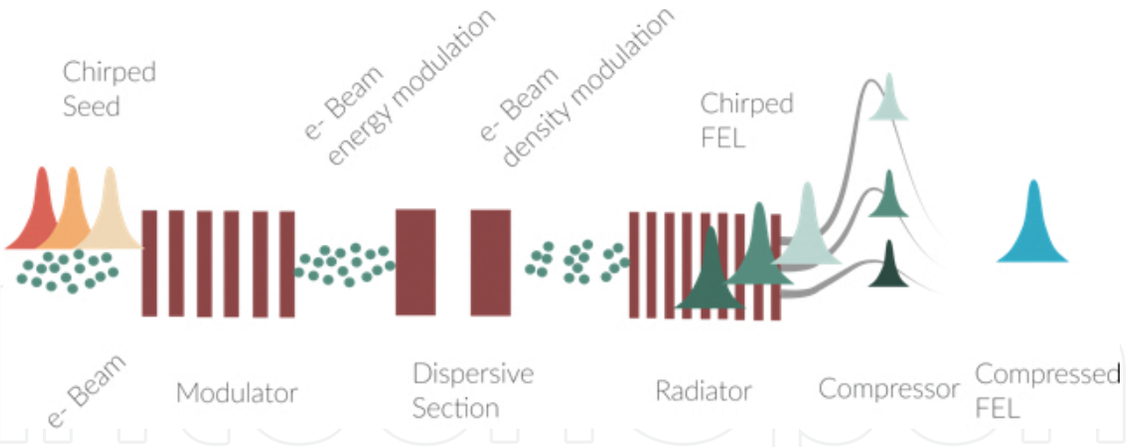

Figure 5. Schematic of the CPA applied to a seeded FEL.

Assuming a linear electron bunch energy spread at the entrance of the FEL radiator, the wavelength spread is evaluated as $\Delta\lambda/\lambda = -2\Delta E/E$. The photon chirp induced by the entrance energy spread is $2\alpha/E$, where α is the electron chirp. This has to be compensated to reduce the pulse time duration.

As a feasibility study, we want to define a configuration to compress an FEL pulse centered at 13.5 nm. **Table 1** resumes the FEL parameters used in the simulation. Using these parameters, the time to be compensated is calculated to be 310 fs for an FEL emission centered at 13.5

nm with a bandwidth $\Delta\lambda$ = 0.8 nm. If the GDD introduced by the compressor is opposite to the intrinsic GDD of the chirped pulse, the pulse time duration is reduced.

Beam energy	0.96 GeV
Charge	0.7 nC
Beam current	1 kA
Bunch duration	270 fs
Energy chirp	−0.15 MeV/ ▪ m

Table 1. FEL parameters used in the simulation.

The compressor parameters are summarized in **Table 2** for the two geometries. The GD of the configurations is shown in **Figure 6(a)**. The curve is almost the same for both geometries. As expected, for narrow-bandwidth pulses, the resulting GD is linear, and the GDD is constant: GDD ≈−37 fs^2.

Pulse central wavelength	13.5 nm
Bandwidth	0.8 nm
Stretching	310 fs
CDG	
Groove density	600 gr/mm
G1-G2 distance	285 mm
Subtended angle	164°
OPG	
Groove density	3600 gr/mm
G1-G2 distance	600 mm
Altitude angle	5°

Table 2. Parameters of the grating compressor in two geometries.

The spatial chirp calculated in the full-width-at-half-maximum (FWHM) bandwidth is 0.9 mm for both geometries. The compressor is typically inserted several tens of meters after the FEL source. As a typical angular divergence of the FEL source at 13.5 nm, 30 μrad (standard deviation) is assumed. The resulting beam diameter at the compressor input, that is assumed to be 50 m far from the source, is 3.6 mm FWHM, therefore much larger than the spatial chirp.

Note that the groove density required in the OPG is higher than the CDG and that the size of the instrument is longer for the OPG. On the basis of the efficiency measurements performed in the two geometries and already discussed in Ref. [54], the total efficiency in the OPG is expected to be higher than the CDG by a factor ≈2.5.

It can be shown that the FEL pulse duration is reduced by a factor of 10 at the output of the compressor, i.e., from 310 fs to about 30 fs. This gives a substantial increase in the temporal resolution of the FEL pulses when used for ultrafast experiments.

4.1. Tunability in wavelength and group delay

The compressor can be tuned in wavelength by rotating the gratings around an axis that is tangent to the surface, passes through the grating center, and is parallel to the grooves. The rotation changes the incidence angle α in the CDG at a constant subtended angle $K = \alpha + \beta$, or the azimuth angle μ in the OPM at constant altitude angle γ. The tuning in wavelength changes also the GD, since it depends on the incidence (azimuth) angles. The delays introduced in the bandwidth $\Delta\lambda$ = 0.8 nm when the central wavelength is tuned in the 10–18 nm interval are shown in **Figure 6(b)**.

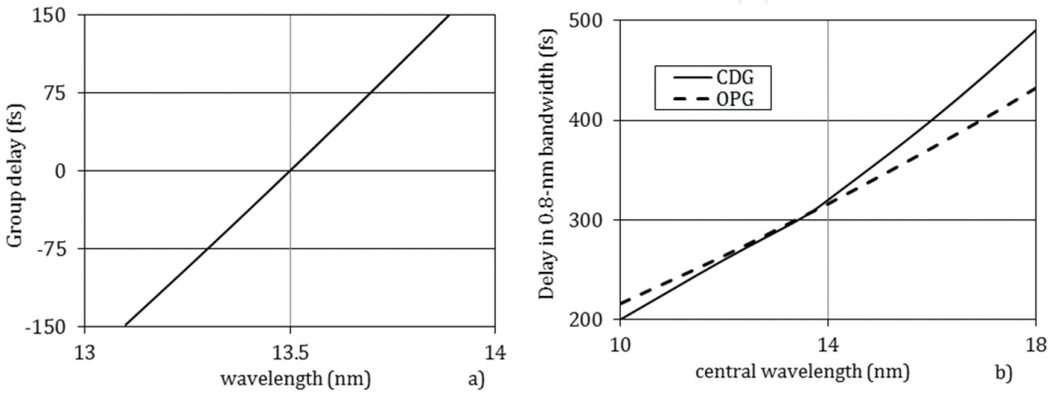

Figure 6. (a) GD of the compressor having the parameters of **Table 2**; (b) change of the delay in the bandwidth when the gratings are rotated to tune the wavelength in the 10–18 nm interval.

It is clear that the simple grating rotation is not sufficient to tune simultaneously the wavelength and the GD. An additional degree of freedom is required that may be the changing of the subtended angle K (the altitude angle γ) in the CDG (OPG), as shown in **Figure 6**. By acting simultaneously on grating rotation and subtended (altitude) angles, users can select simultaneously the wavelength and GD. This makes the design very flexible.

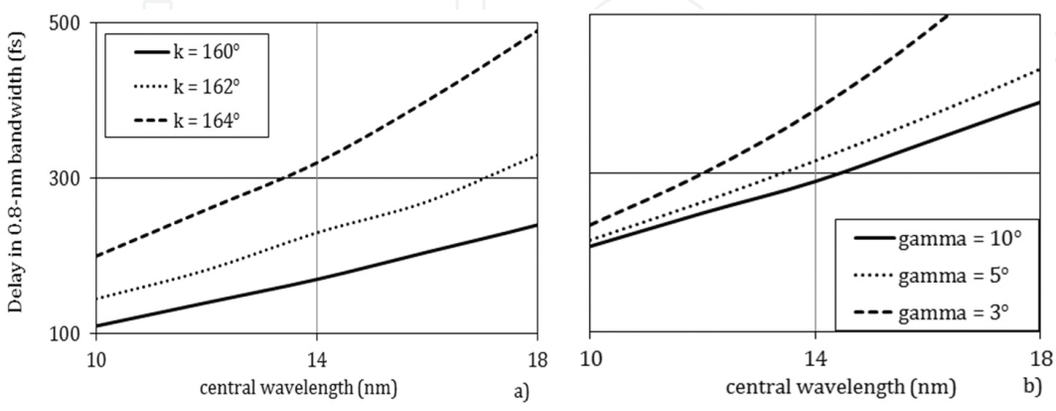

Figure 7. Delay in 0.8-nm bandwidth introduced by the compressor having the parameters of **Table 2** when the gratings are rotated to tune the wavelength in the 10–18 nm interval: (a) CDG, variable subtended angle; (b) OPG, variable altitude angle.

The optical setup of the compressor is shown in **Figure 7**. The instrument consists of two plane gratings and two plane mirrors. The two mirrors are used to deviate the FEL beam in the same direction as the input.

4.2. Operation with a diverging beam

The formulas calculated above assume to work with a collimated beam. In this case, the number of illuminated groove is the same for the two gratings when they are parallel, giving a corrected pulse-front tilt at the output. Indeed, in the real case of an FEL-divergent beam, this would require the use of an additional mirror at the input of the compressor to collimate the beam, namely a grazing-incidence parabola that makes the design complex. Indeed, the compressor, as presented in the previous paragraph, can be used in a divergent beam if the second grating is operated slightly out from the parallel condition, to have the same number of illuminated grooves.

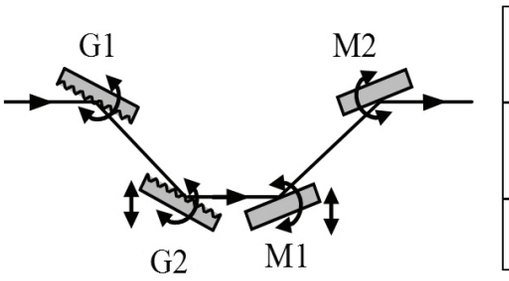

G1 rot	wavelength scanning change of angle K
G2 rot-tra	wavelength scanning change of angle K
M1 rot-tra *M2 rot*	deviation of the beam

(a)

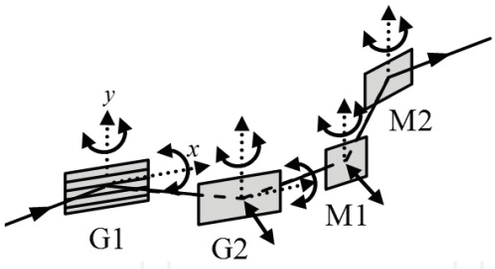

G1 rot	wavelength scanning change of altitude
G2 rot-tra	wavelength scanning change of altitude

(b)

Figure 8. Optical setup of the compressor: (a) CDG; (b) OPG.

The geometry with a divergent beam is shown in **Figure 8** for CDG. The number of illuminated grooves is the same for both gratings if G2 is operated at a lower subtended angle, $k_2 < k_1$:

$$\cos\alpha_2 = \cos\beta_1 + \frac{q_{CD}\delta_1}{S_1}\frac{\cos^2\alpha_1}{\cos\beta_1} \tag{9}$$

where δ_1 is the divergence of the incoming beam, S_1 is the beam cross section at G1, α_1 and β_1 the incidence and diffraction angles on G1, and α_2 the incidence angle on G2.

In the case of OPM, the compensation of the pulse-front tilt is expressed by

$$\cos\mu_2 = \cos\mu_1 + \frac{q_{OP}\delta_1}{S_1} \tag{10}$$

where μ_1 and μ_2 are the azimuth angles on G1 and G2.

The asymmetry between G1 and G2 depends on the actual divergence of the FEL beam and on the distance between the two gratings. Let us assume the parameters of **Table 2**, with 30-μrad divergence (standard deviation). The compressor stage is supposed to be installed 50 m far from the source. In the case of CDG, the residual pulse-front tilt at 13.5 nm is 5 fs FWHM if the gratings are operated parallel and the correction to be applied to α_2 is 0.1°. If the compressor is used at longer wavelengths, the asymmetry to be applied is more remarkable because of the higher FEL divergence.

The spatial chirp, that does not influence the quality of the final spot size in case of a parallel beam, has to be evaluated in case of a divergent beam, since different wavelengths are focused in different points in the direction of the spectral dispersion. This gives a slight asymmetry in the spot profile that is broadened in the direction of spectral dispersion. Let us define M as the total demagnification of the FEL beamline, $M \approx 50$–100. The spatial chirp SC gives a limit to the minimum focal spot that can be achieved in the direction of the spectral dispersion, as SC/M. Assuming the same parameters of **Table 2** and $M = 75$, the minimum spot size that can be achieved in the direction of the spectral dispersion is 12 μm FWHM. The broadening due to the spatial chirp is generally negligible for spot sizes in the 20–50 μm range. However, the use of the compressor may degrade the quality of the final focus if the beamline is tailored to give micro-focusing. In such cases, the insertion of the compressor has to be carefully evaluated.

4.3. Efficiency of the compressor

The efficiency of the compressor depends on the geometry adopted for the gratings, since it is well known that the OPG gives efficiency higher than the CDG [59].

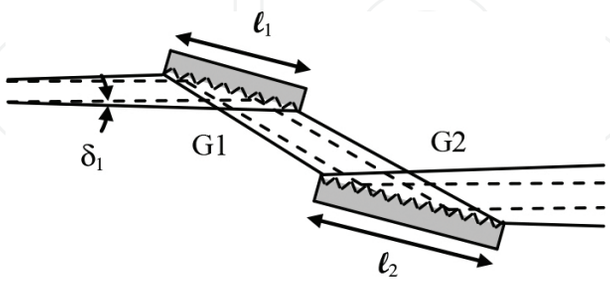

Figure 9. Grating compressor operated in divergent beam. The pulse-front tilt is corrected for $l_2 = l_1$.

To compare the two geometries, the first-order diffraction efficiency has been measured in the 25–35 nm (35–50 eV) region in the two different geometries. Both gratings are plane, gold-coated, and have 600 gr/mm groove density. The grating used in the CDG is blazed at 2°, and the grating used in the OPG is blazed at 7°. The results are shown in **Figure 9**. The efficiency

in the OPG is a factor ≈2 higher than the CDG that gives a factor 4 in the total efficiency of the compressor. The latter is expected to be ≈5% in the CDG and ≈20% in the OPG [60].

5. Grating compressor for attosecond pulses

Attosecond pulses generated with the scheme of HHs by the use of laser pulses of few optical cycles are positively chirped as a result of the different duration of the quantum paths that contribute to the different portions of the emitted spectrum. They can be compressed by introducing a suitable device with a negative GDD.

The simplest device that exhibits negative GDD is a thin metallic filter. Anomalous dispersion near absorption resonances can be exploited to compensate the positive chirp of the generated attosecond pulses. Aluminum or zirconium is normally used in the XUV range, depending on the spectral range of operation [61]. Furthermore, the filter is also useful to block the IR laser beam since it is totally solar blind. The main drawback of the filter is the strong XUV absorption that may even exceed one order of magnitude.

Aperiodic multilayer mirrors have also been developed and successfully tested for the dispersion control in the XUV [62–65]. The multilayer coating is designed to compensate for the attosecond chirp and reduce the pulse duration. Pulse compression and focusing are demanded to the same optical element that makes the design simple and compact. For a center-photon energy range of 100–120 eV, the mirror reflectivity is approximately 10% and the bandwidth 10–13 eV. Recently, also mirrors for the water-window region have been tested, although with reflectivity lower than 1% [66]. A metallic filter has to be inserted anyway in the optical path to block the IR laser light.

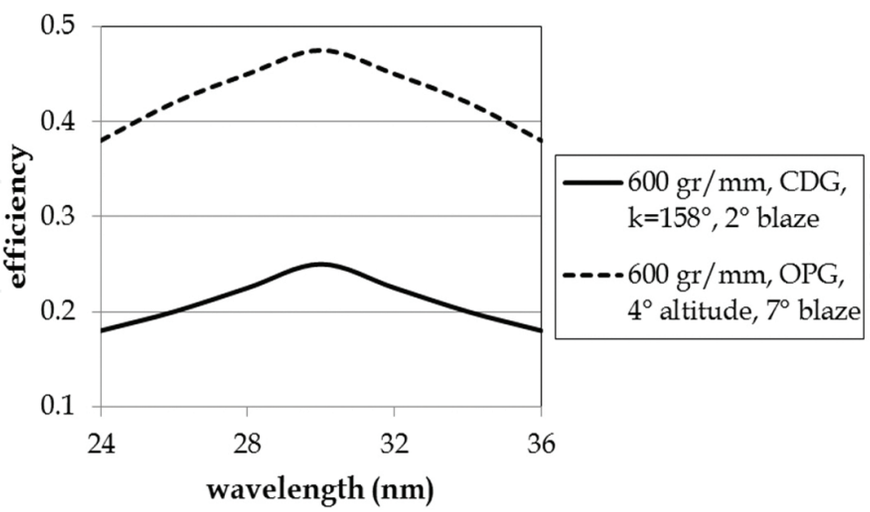

Figure 10. Comparison of efficiencies measured in CDG and OPG.

We discuss here the use of gratings to compress attosecond pulses by introducing a GDD that compensates for the intrinsic pulse chirp. Unfortunately, the configuration with plane gratings

discussed above is not suitable, since the G1-to-G2 distance q that is required to give the necessary GDD is too small to be realized in practice. Therefore, the plane-grating configuration has to be modified as shown in **Figure 10** for the OPG [67, 68], by adding an intermediate focal point between the two gratings. The case of CDG is analogous.

The design consists of six optical elements: four identical grazing incidence parabolic mirrors (P1-P4) and two identical plane gratings (G1, G2). The XUV source is located in the front focal plane of P1, and the rays are collected at the focus of the last parabolic mirror P4. The parabolic mirrors are used to collimate and refocus the XUV radiation with negligible aberrations, and the gratings are illuminated in parallel light. A spectrally dispersed image of the source is obtained in the intermediate plane. The two focusing mirrors placed between the gratings act as a telescopic arrangement. Differently from the plane-grating compressor discussed above, this makes it possible to: (i) continuously tune the GDD from negative to positive values and (ii) achieve the exceedingly small grating separations necessary to compensate the attosecond chirp.

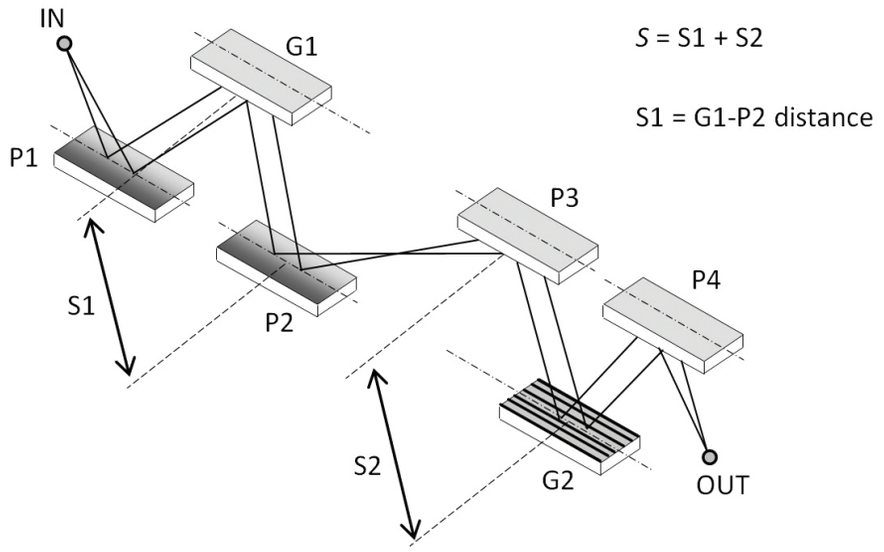

Figure 11. Grating compressor for attosecond pulses.

With reference to the symbols listed in **Figure 11**, the condition for zero GDD is to have G1 imaged on G2, that is realized when $S1 + S2 = 2f$. Since f is fixed, the GDD depends on $S1 + S2$: for $S1 + S2 < 2f$, G1 is imaged behind G2, and the resulting GDD is positive; for $S1 + S2 > 2f$, G1 is imaged before G2, and the resulting GDD is negative. Once the equivalent distance q that is required for compensation has been calculated, the effective displacement from the zero-dispersion case is $\Delta S = q/(\omega_0 \sin\gamma \cos\nu)$, where ω_0 is the center angular frequency. It can be noted that the design of the compressor is simplified if $S1$ is kept fixed, and only $S2$ is tuned to change the GDD. A suitable value for f is in the range of 200–300 mm, giving a total length of the compressor of ≈1.5 m.

As an application to ultrashort pulses, a compressor design for the 50–100 eV region is discussed here. The characteristics of the compressor are resumed in **Table 3**. The GD

introduced with the distance $S = S1 + S2$ is shown in **Figure 12**. An example of compression of a pulse with a positive GDD is presented in **Figure 13**, adapted from [69]. Note that the chirp introduced by the compressor is able to compensate the pulse chirp down to a nearly single-cycle pulse (**Figure 14**).

Pulse spectral interval	50-100 eV, 12-24 nm
Mirrors	**Off-axis parabola**
Input/output arms	300 mm
Grazing angle	3°
Gratings	**Plane**
Groove density	200 gr/mm
Altitude angle	1.5°
Distances	S1+S2 > 600 mm for negative GDD

Table 3. Parameters of the compressor for the 50–100 eV region.

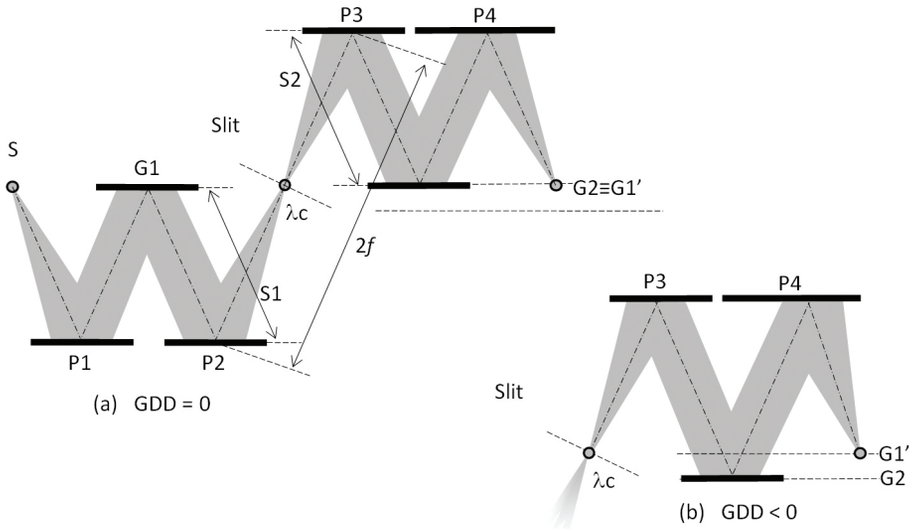

Figure 12. Operation of the attosecond compressor: (a) GDD = 0; (b) GDD < 0.

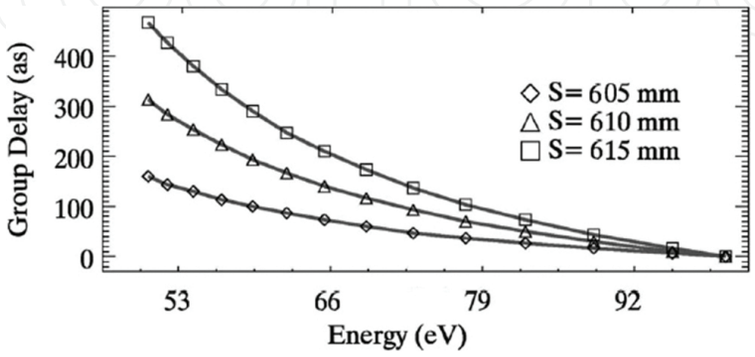

Figure 13. GD of the compressor with parameters listed in **Table 3**.

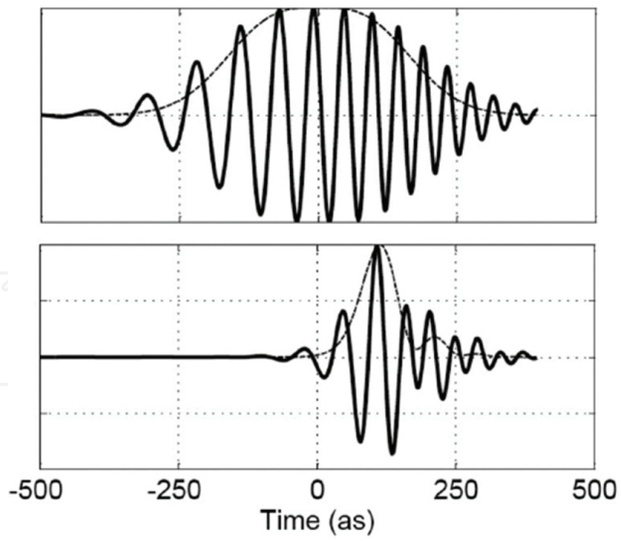

Input pulse: central energy 73 eV, bandwidth 25 eV, GDD = +5100 as².

Compressor: *S1*+*S2* = 610 mm.

Figure 14. Simulation of the compression of a XUV pulse with the parameters of **Table 3**.

5.1. Example of application to attosecond pulses

A schematic view of an experiment using compressed attosecond pulses is shown in **Figure 15**. The XUV attosecond pulses are generated on a gas jet in a vacuum chamber and are intrinsically chirped. The XUV radiation is generated with the intrinsic attosecond chirp. Different wavelengths travel in different paths inside the compressor that compensates for the chirp and reduces the time duration of the pulse.

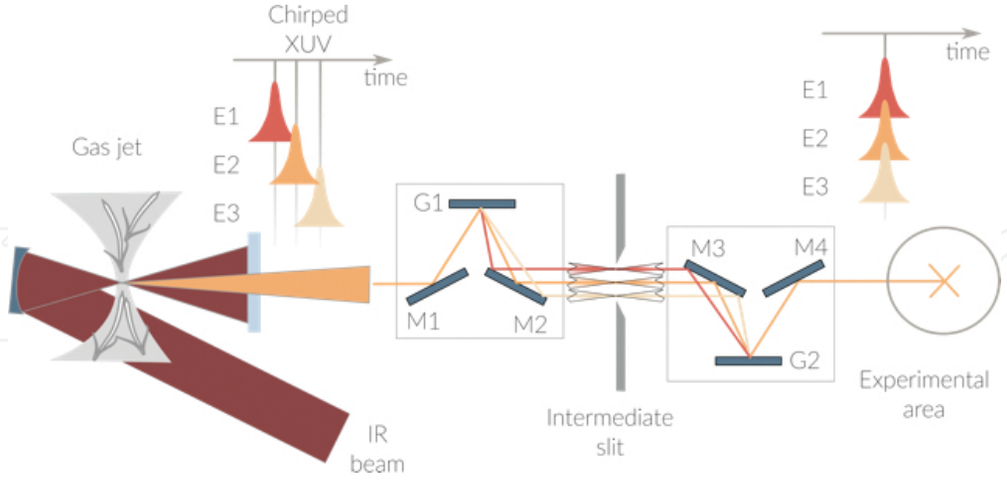

Figure 15. Schematic of the attosecond compressor.

Attosecond pulses are generated in different XUV spectral windows, depending on the interacting gas. Using argon and ≈$2 \cdot 10^{14}$ W/cm² ultrafast laser intensity, radiation is generated in the 25–55 eV region, while with neon and ≈$6 \cdot 10^{14}$ W/cm² intensity, radiation is generated in the 50–120 eV region. Attosecond pulses are generated from the short trajectory

components, since this is the part of the generated radiation that survives propagation in the generating medium. Aluminum and zirconium filters can be used, respectively, in the low- (i.e., argon) and high-energy range (i.e., neon) to introduce negative chirp to compensate for the intrinsic chirp of the attosecond pulses and compress them close to the Fourier limit.

Here, we discuss the parameters to be used for a grating compressor in the two different XUV regions. For the lower intensity case, the parameters are $\sigma = 100$ grooves/mm, $\gamma = 1.5°$, $\mu = 3.7°$, $\Delta S = 23$ mm. For the higher intensity case, the parameters are $\sigma = 200$ grooves/mm, $\gamma = 1°$, $\mu = 4.1°$, $\Delta S = 29$ mm.

Simulations of the generated and compressed pulses have been performed starting from 25-fs driving pulses at 790 nm [70]. The generated pulses have a duration of 270 as in argon and 200 in neon, while the Fourier-limited duration would be, respectively, 115 and 35 as. At the output of the grating compressor, the pulse duration results, respectively, 160 and 60 as, much closer to the Fourier limit. It is also shown that the optimal Al filter would reduce the pulse duration to 130 as, therefore shorter than the grating compressor, while the optimal Zr filter would reduce the pulse duration to 90 as, therefore longer than the grating compressor.

In general, the grating compressor is more versatile than metal filters and can be continuously tuned from negative to positive GDD with constant throughput.

6. Conclusions

The use of diffraction gratings to manipulate the spectral phase of XUV ultrashort pulses has been discussed. The system consists of two gratings to introduce the required phase chirp. Both the classical and the off-plane geometries have been discussed.

Both a simple design with two plane gratings working in collimated beam and a more complex design with two plane gratings and an intermediate focal point have been discussed. Both designs are tunable in wavelength range to cover the whole spectral extension of the source and operate at different wavelengths; furthermore, once the operating wavelength has been chosen, the GDD is tunable to compensate for the actual pulse chirp.

The use of elements at grazing incidence makes the system particularly suitable for the application to CPA of intense FEL pulses and to compression of attosecond pulses, playing an important role for the photon handling and conditioning of future ultrashort sources.

Acknowledgements

The results discussed here have been partially funded by Extreme Light Infrastructures (ELI) funds of the Italian Ministry for Education, University and Research.

Author details

Fabio Frassetto, Paolo Miotti and Luca Poletto*

*Address all correspondence to: luca.poletto@ifn.cnr.it

CNR-Institute of Photonics and Nanotechnologies, Padova, Italy

References

[1] Diels J-C, Rudolph W. Ultrashort Laser Pulse Phenomena. Oxford: Academic Press Inc.; 2006.

[2] Jaegle' P. Coherent Sources of XUV Radiation. Berlin: Springer; 2006.

[3] Marciak-Kozlowska J. From Femto-to Attoscience and Beyond. New York: Nova Science Publishers Inc; 2009.

[4] Vrakking M J J, Elsaesser T. X-Ray Photonics: X-rays Inspire Electron Movies. Nat. Photonics. 2012;6:645–647.

[5] Lépine F, Ivanov M Y, Vrakking, M J J. Attosecond Molecular Dynamics: Fact or Fiction?. Nat. Photonics. 2014;8:195–204.

[6] Canova F, Poletto L, editors. Optical Technologies for Extreme-Ultraviolet and Soft X-ray Coherent Sources. Berlin: Springer; 2015.

[7] Chang Z, Rundquist A, Wang H, Murnane M M, Kapteyn H C. Generation of Coherent Soft X Rays at 2.7 nm Using High Harmonics. Phys. Rev. Lett. 1997;79:2967–2970.

[8] Schnürer M, Spielmann Ch, Wobrauschek P, Streli C, Burnett N H, Kan C, Ferencz K, Koppitsch R, Cheng Z, Brabec T, Krausz F. Coherent 0.5-keV X-Ray Emission from Helium Driven by a Sub-10-fs Laser. Phys. Rev. Lett. 1998;80:3236–3239.

[9] Takahashi E J, Kanai T, Ishikawa K L, Nabekawa Y, Midorikawa K. Coherent Water Window X Ray by Phase-Matched High-Order Harmonic Generation in Neutral Media. Phys. Rev. Lett. 2008;101:253901.

[10] Corkum P, Krausz F. Attosecond Science. Nat. Physics. 2007;3:381–387.

[11] Krausz F, Ivanov M. Attosecond Physics. Rev. Mod. Phys. 2009;81:163–234.

[12] Sansone G, Poletto L, Nisoli M. High-Energy Attosecond Light Sources. Nat. Photonics. 2011;5:655–663.

[13] Krausz F, Stockman M I. Attosecond metrology: from electron capture to future signal processing. Nat. Photonics. 2014;8:205–213.

[14] Paul P M, Toma E S, Breger P, Mullot G, Auge F, Balcou P, Muller H G, Agostini P. Observation of a Train of Attosecond Pulses from High Harmonic Generation. Science. 2001;292:1689–1692.

[15] Lopez-Martens R, Varju K, Johnsson P, Mauritsson J, Mairesse Y, Salières P, Gaarde M B, Schafer K J, Persson A, Svanberg S, Wahlström C-G, L'Huillier A. Amplitude and Phase Control of Attosecond Light Pulses. Phys. Rev. Lett. 2005;94:033001.

[16] Kienberger R, Goulielmakis E, Uberacker M, Baltuska A, Yakovlev V, Bammer F, Scrinzi A, Westerwalbesloh T, Kleineberg U, Heinzmann U, Drescher M, Krausz F. Atomic Transient Recorder. Nature. 2004;427:817–822.

[17] Sansone G, Benedetti E, Calegari F, Vozzi C, Avaldi L, Flammini R, Poletto L, Villoresi P, Altucci C, Velotta R, Stagira S, De Silvestri S, Nisoli M. Isolated Single-Cycle Attosecond Pulses. Science. 2006;314:443–446.

[18] Zhao K, Zhang Q, Chini M, Wu Y, Wang X, Chan Z. Tailoring a 67 Attosecond Pulse Through Advantageous Phase-Mismatch. Opt. Lett. 2012;37:3891–3893.

[19] Chini M, Zhao K, Chang Z. The Generation, Characterization and Applications of Broadband Isolated Attosecond Pulses. Nat. Photonics. 2014;8:178–186.

[20] Mairesse Y, de Bohan A, Frasinski L J, Merdji H, Dinu L C, Monchicourt P, Breger P, Kovacev M, Auguste T, Carré B, Muller H G, Agostini P, Salières P. High-Harmonics Chirp and Optimization of Attosecond Pulse Trains. Laser Phys. 2005;15:863–870.

[21] Schultze M, Goulielmakis E, Uiberacker M, Hofstetter M, Kim J, Kim D, Krausz F, Kleineberg U. Powerful 170-Attosecond XUV Pulses Generated with Few-Cycle Laser Pulses and Broadband Multilayer Optics. New J. Phys. 2007;9:243–253.

[22] Saldin E L, Schneidmiller E A, Yurkov M V. The Physics of Free Electron Lasers. Berlin: Springer; 2000.

[23] Ding Y, Decker F-J, Emma P, Feng C, Field C, Frisch J, Huang Z, Krzywinski J, Loos H, Welch J, Wu J, Zhou F. Femtosecond X-Ray Pulse Characterization in Free-Electron lasers Using a Cross-Correlation Technique. Phys. Rev. Lett. 2012;109:254802.

[24] Emma P J, Bane K, Cornacchia M, Huang Z, Schlarb H, Stupakov G, Nalz D. Femtosecond and Sub-femtosecond X-Ray Pulses from a Self-Amplified Spontaneous-Emission–Based Free-Electron Laser. Phys. Rev. Lett. 2004;92:074801.

[25] Ding Y, Huang Z, Ratner D, Bucksbaum P, Merdji H. Generation of Attosecond X-Ray Pulses with a Multicycle Two-Color Enhanced Self-Amplified Spontaneous Emission Scheme. Phys. Rev. ST Accel. Beams. 2009;12:060703.

[26] Tanaka T. Proposal for a Pulse-Compression Scheme in X-Ray Free-Electron Lasers to Generate a Multiterawatt, Attosecond X-Ray Pulse. Phys. Rev. Lett. 2013;110:084801.

[27] Rosenzweig J B, Alesini D, Andonian G, Boscolo M, Dunning M, Faillace L, Ferrario M, Fukusawa A, Giannessi L, Hemsing E, Marcus G, Marinelli A, Musumeci P, O'Shea B,

Palumbo L, Pellegrini C, Petrillo V, Reiche S, Ronsivalle C, Spataro B, Vaccarezza C. Generation of Ultra-Short, High Brightness Electron Beams for Single-Spike SASE FEL Operation. Nucl. Instrum. Meth. A. 2008;593:39–44.

[28] Shu X, Peng T, Dou Y. Chirped Pulse Amplification in a Free-Electron Laser Amplifier. J. Elect. Spect. Rel. Phen. 2011;184:350–353.

[29] Feng C, Shen L, Zhang M, Wang D, Zhao Z, Xian D. Chirped Pulse Amplification in a Seeded Free-Electron Laser for Generating High-Power Ultra-Short Radiation. Nucl. Inst. Meth. Phys. Res. A. 2013;712:113–119.

[30] Poletto L, Tondello G, Villoresi P. High-order Laser Harmonics Detection in the EUV and Soft X-Ray Spectral Regions. Rev. Sci. Instr. 2001;72:2868–2874.

[31] Poletto L, Bonora S, Pascolini M, Villoresi P. Instrumentation for Analysis and Utilization of Extreme-Ultraviolet and Soft X-Ray High-order Harmonics. Rev. Sci. Instr. 2004;75:4413–4418.

[32] Frassetto F, Cacho C, Froud C, Turcu I C E, Villoresi P, Bryan W A, Springate E, Poletto L. Single-Grating Monochromator for Extreme-Ultraviolet Ultrashort Pulses. Opt. Express. 2011;19:19169–19181.

[33] Grazioli C, Callegari C, Ciavardini A, Coreno M, Frassetto F, Gauthier D, Golob D, Ivanov R, Kivimäki A, Mahieu B, Bučar B, Merhar M, Miotti P, Poletto L, Polo E, Ressel B, Spezzani C, De Ninno G. CITIUS: An Infrared-Extreme Ultraviolet Light Source for Fundamental and Applied Ultrafast Science. Rev. Sci. Instrum. 2014;85:023104.

[34] Poletto L, Miotti P, Frassetto F, Spezzani C, Grazioli C, Coreno M, Ressel B, Gauthier D, Ivanov R, Ciavardini A, de Simone M, Stagira S, De Ninno G. Double-Configuration Grating Monochromator for Extreme-Ultraviolet Ultrafast Pulses. Appl. Opt. 2014;53:5879–5888.

[35] Ojeda J, Arrell C A, Grilj J, Frassetto F, Mewes L, Zhang H, van Mourik F, Poletto L, Chergui M. Harmonium: A Pulse Preserving Source of Monochromatic EUV (30–110 eV) Radiation for Ultrafast Photoelectron Spectroscopy of Liquids. Structural Dynamics. 2016;3:023602.

[36] Martins M, Wellhöfer M, Hoeft J T, Wurth W, Feldhaus J, Follath R. Monochromator Beamline for FLASH. Rev. Sci. Inst. 2006;77:115108.

[37] Guerasimova N, Dziarzhytski S, Feldhaus J. The Monochromator Beamline at FLASH: Performance, Capabilities and Upgrade Plans. J. Mod. Opt. 2011;58:1480–1485.

[38] Heimann P, Krupin O, Schlotter W F, Turner J, Krzywinski J, Sorgenfrei F, Messerschmidt M, Bernstein D, Chalupský J, Hájková V, Hau-Riege S, Holmes M, Juha L, Kelez N, Lüning J, Nordlund D, Fernandez Perea M, Scherz A, Soufli R, Wurth W, Rowen M. Linac Coherent Light Source Soft X-Ray Materials Science Instrument Optical Design and Monochromator Commissioning. Rev. Sci. Inst. 2011;82:093104.

[39] Schlotter W F, Turner J J, Rowen M, Heimann P, Holmes M, Krupin O, Messerschmidt M, Moeller S, Krzywinski J, Soufli R, Fernández-Perea M, Kelez N, Lee S, Coffee R, Hays G, Beye M, Gerken N, Sorgenfrei F, Hau-Riege S, Juha L, Chalupsky J, Hajkova V, Mancuso A P, Singer A, Yefanov O, Vartanyants I A, Cadenazzi G, Abbey B, Nugent K A, Sinn H, Lüning J, Schaffert S, Eisebitt S, Le W-S, Scherz A, Nilsson A R, Wurth W. The Soft X-Ray Instrument for Materials Studies at the Linac Coherent Light Source X-Ray Free-Electron Laser. Rev. Sci. Inst. 2012;83:043107.

[40] Poletto L, Frassetto F. Time-Preserving Monochromators for Ultrafast Extreme-Ultraviolet Pulses. Appl. Opt. 2010;49:5465–5473.

[41] Villoresi P. Compensation of Optical Path Lengths in Extreme-Ultraviolet and Soft-X-Ray Monochromators for Ultrafast Pulses. Appl. Opt. 1999;38:6040–6049.

[42] Poletto L. Time-Compensated Grazing-Incidence Monochromator for Extreme-Ultraviolet and Soft X-Ray High-order Harmonics. Appl. Phys. B. 2004;78:1013–1016.

[43] Poletto L, Villoresi P. Time-Compensated Monochromator in the Off-Plane Mount for Extreme-Ultraviolet Ultrashort Pulses. Appl. Opt. 2006;45:8577–8585.

[44] Poletto L, Villoresi P, Benedetti E, Ferrari F, Stagira S, Sansone G, Nisoli M. Intense Femtosecond Extreme Ultraviolet Pulses by Using a Time-Delay Compensated Monochromator. Opt. Lett. 2007;32:2897–2899.

[45] Poletto L, Villoresi P, Frassetto F, Calegari F, Ferrari F, Lucchini M, Sansone G, Nisoli M. Time-Delay Compensated Monochromator for the Spectral Selection of Extreme-Ultraviolet High-order Laser Harmonics. Rev. Sci. Instrum. 2009;80:123109.

[46] Ito M, Kataoka Y, Okamoto T, Yamashita M, Sekikawa T. Spatiotemporal Characterization of Single-order High Harmonic Pulses from Time-Compensated Toroidal-Grating Monochromator. Opt. Express. 2010;18:6071–6078.

[47] Igarashi H, Makida A, Ito M, Sekikawa T. Pulse compression of Phase-Matched High Harmonic Pulses from a Time-Delay Compensated Monochromator. Opt. Express. 2012;20:3725–3732.

[48] Poletto L, Azzolin P, Tondello G. Beam-Splitting and Recombining of Free-Electron-Laser Extreme-Ultraviolet Radiation. Appl. Phys. B. 2004;78:1009–1011.

[49] Frassetto F, Villoresi P, Poletto L. Beam Separator for High-Order Harmonic Radiation in the 3–10 nm Spectral Region. J. Opt. Soc. Am. A. 2008;25:1104–1114.

[50] Poletto L, Frassetto F, Villoresi P. Ultrafast Grating Instruments in the Extreme Ultraviolet. IEEE J. Sel. Top. Quantum Electron. 2012;18:467–478.

[51] Werner W. X-Ray Efficiencies of Blazed Gratings in Extreme Off-Plane Mountings. Appl. Opt. 1977;16:2078–2080.

[52] Petit R. Electromagnetic Theory of Gratings. Berlin: Springer; 1980.

[53] Werner W, Visser H. X-Ray Monochromator Designs Based on Extreme Off-Plane Grating Mountings. Appl. Opt. 2006;20:487–492.

[54] Pascolini M, Bonora S, Giglia A, Mahne N, Nannarone S, Poletto L. Gratings in the Conical Diffraction Mounting for an EUV Time-Delay Compensated Monochromator. Appl. Opt. 2006;45:3253–3562.

[55] Martinez O. 3000 Times Grating Compressor with Positive Group Velocity Dispersion: Application to Fiber Compensation in 1.3–1.6 μm Region. IEEE J. Quantum Electron. 1987;23:59–64.

[56] Martinez O. Design of High-Power Ultrashort Pulse Amplifiers by Expansion and Recompression. IEEE J. Quantum Electron. 1987;23:1385–1387.

[57] Frassetto F, Poletto L. Grating Configurations to Compress Extreme-Ultraviolet Ultrashort Pulses. Appl. Opt. 2015;54:7985–7992.

[58] Frassetto F, Giannessi L, Poletto L. Compression of XUV FEL Pulses in the Few-Femtosecond Regime. Nucl. Instr. Meth. A. 2008;593:14–16.

[59] Poletto L, Bonora S, Pascolini M, Borgatti F, Doyle B, Giglia A, Mahne N, Pedio M, Nannarone S. Efficiency of Gratings in the Conical Diffraction Mounting for an EUV Time-Compensated Monochromator. In: Proc. SPIE Vol. 5534 Fourth Generation X-Ray Sources and Optics II; August 2004; Denver (USA). SPIE Publisher; 2004. p. 144–153.

[60] Poletto L, Frassetto F, Miotti P, Gauthier D, Fajardo M, Mahieu B, Svetina C, Zangrando M, Zeitoun P, De Ninno G. Grating-Based Pulse Compressor for Applications to FEL Sources. In: Proc. SPIE Vol. 9512, Advances in X-ray Free-Electron Lasers Instrumentation; April 2015; Prague (Czech Rep.). SPIE Publisher; 2015. p. 951210.

[61] Sola J, Mevel E, Elouga L, Constant E, Strelkov V, Poletto L, Villoresi P, Benedetti E, Caumes J-P, Stagira S, Vozzi C, Sansone G, Nisoli M. Controlling Attosecond Electron Dynamics by Phase-Stabilized Polarization Gating. Nat. Phys. 2006;2:319–322.

[62] Morlens A-S, Lopez-Martens R, Boyko O, Zeitoun P, Balcou P, Varju K, Gustafsson E, Remetter T, L'Huillier A, Kazamias S, Gautier J, Delmotte F, Ravet M-F. Design and Characterization of Extreme Ultraviolet Broadband Mirrors for Attosecond Science. Opt. Lett. 2006;31:1558–1560.

[63] Suman M, Monaco G, Pelizzo M-G, Windt D L, Nicolosi P. Realization and Characterization of an XUV Multilayer Coating for Attosecond Pulses. Opt. Express. 2009;17:7922–7932.

[64] Hofstetter M, Schultze M, Fie M, Dennhardt B, Guggenmos A, Gagnon J, Yakovlev V S, Goulielmakis E, Kienberger R, Gullikson E M, Krausz F, Kleineberg U. Attosecond Dispersion Control by Extreme Ultraviolet Multilayer Mirrors. Opt. Express. 2011;19:1767–1776.

[65] Bourassin-Bouchet C, de Rossi S, Wang J, Meltchakov E, Giglia A, Mahne N, Nannarone S, Delmotte F. Shaping of Single-Cycle Sub-50-Attosecond Pulses with Multilayer Mirrors. New J. Phys. 2012;14:023040.

[66] Guggenmos A, Rauhut R, Hofstetter M, Hertrich S, Nickel B, Schmidt J, Gullikson E M, Seibald M, Schnick W, Kleineberg U. Aperiodic CrSc Multilayer Mirrors for Attosecond Water Window Pulses. Opt. Express. 2013;21:21728–21740.

[67] Frassetto F, Villoresi P, Poletto L. Optical Concept of a Compressor for XUV Pulses in the Attosecond Domain. Opt. Express. 2008;16:6652–6667.

[68] Poletto L, Frassetto F, Villoresi P. Design of an Extreme-Ultraviolet Attosecond Compressor. J. Opt. Soc. Am. B. 2008;25:B133–B136.

[69] Poletto L, Villoresi P, Frassetto F. Diffraction Gratings for the Selection of Ultrashort Pulses in the Extreme-Ultraviolet. In: M. Grishin, editor. Advances in Solid-State Lasers: Development and Applications. INTECH, Croatia; 2010. p. 413–438.

[70] Mero M, Frassetto F, Villoresi P, Poletto L, Varju K. Compression Methods for XUV Attosecond Pulses. Opt. Express. 2011;19:23420–23428.

IntechOpen